scientific reports

Check for updates

OPEN

A novel tube law analysis under anisotropic external load

Lorenzo Lotti[1], Costanza Carbonari[1]✉, Giulio Calvani[2] & Enio Paris[1]

Mathematical and physical modeling of flows in collapsible pipes often relates the flow area to the difference between the internal and the external pressures (i.e. the transmural pressure). The relation is used to model the conduits of the human body transporting biological fluids, is called tube law and usually considers the transmural pressure resulting from isotropic external pressure only. We provide a new empirical tube law considering anisotropic conditions of the external load; our formulation is based on the hypothesis, supported by clinical and experimental findings, that in physiological conditions both isotropic and anisotropic stresses are combined in the external load acting on vessels. The proposed mathematical model was validated through laboratory experiments reproducing the flow through a collapsible tube representing the physiological conditions of male urethra during micturition. The proposed tube law better agrees with the experimental observations, in comparison to classic formulations available in literature, thus showing that the proposed model better describes the physiological condition of flow in collapsible tubes subjected to anisotropic external load. The application of our model can be readily extended to several types of vessels.

Keywords Anisotropic load, Collapsible-tube flow, Tube law

Most fluid-conveying vessels in humans are largely flexible and present elastic deformation in response to stresses exerted by the fluid and the confining/surrounding tissues. Usually, the elastic deformation of such vessels is modelled by considering the transmural pressure, defined as the difference between the intraluminal pressure characterizing the flow and the external stress acting on the outer surface of the vessel. For large positive values of the transmural pressure, the tube is inflated and rather stiff since an increase of the cross-section requires the perimeter to be stretched[1,2]. When the transmural pressure is lower than a critical value, such elastic vessels can buckle[3]. For large negative values of the transmural pressure the tube collapses to two small lumina separated by a flat contact zone of opposite walls[4,5], the tube being in this case rather stiff, as well.

In between these two stiff configurations the tube is highly compliant undergoing large cross-section changes for small pressure variations given that only wall bending is needed for shape change[1]. Although inflated vessels represent the majority of cases in the human body, many relevant exceptions are present (for a comprehensive review the reader is referred to[2]): some examples are coronary arteries during systole[6]; arteries actively compressed, as occurs during blood-pressure-measuring; veins above the heart level because of the gravitational pressure drop with height[7]; large intrathoracic airways during expiration from the lung[8–10]; the urethra during micturition[11].

Given the physiological and clinical relevance of such buckled and collapsed vessels situations and associated phenomena, the topic has been and is largely addressed by both experimental research and mathematical and numerical analyses. The simple and widespread physical model used for such investigations is the experimental setup named "Starling Resistor"[12], an elastic tube mounted on two rigid tubes enclosed by a pressure chamber whose pressure is independently controlled, the control variables of the system being the pressures immediately upstream and downstream the elastic tube, the external hydrostatic pressure, and the flow rate. In particular, the Starling Resistor has been used to study elastic jump[13], self-excited oscillations[14,15], wave propagation[16], pressure-drop limitation[14,17]and flow limitation[18], this last being a maximum critical value of flow rate caused by tube collapse.

Flow limitation has been the major motivation for a mathematical understanding and representation of collapsible-tube flows. The simplest mathematical model of collapsible-tube flows consists of the one-dimensional continuity and momentum equations coupled with a third equation, referred as "tube law" relating cross-sectional area with transmural pressure[19,20]. The key feature of this relationship is that the tube is inflated and with a circular cross-section for null and positive transmural pressure, whereas it is deformed or collapsed for negative transmural pressure[19].

[1]Department of Civil and Environmental Engineering, University of Florence, Via di S. Marta, 3, Florence 50139, Italy. [2]Platform of Hydraulic Constructions, Swiss Federal Institute of Technology of Lausanne, GC A3 505 Station 18, Lausanne 1015, Switzerland. ✉email: costanza.carbonari@unifi.it

However, experimental observations attested deformed, elliptical cross-sections for null transmural pressure in compliant polymeric tubes[21–24]; other experimental studies indicate that in some cases arteries and veins can have a not circular, deformed and buckled cross-section for positive transmural pressure, as it is the case of canine carotid arteries and jugular veins for physiologically relevant pressure ranges[25]. Further experimental evidence attests that some human vessels have a slit-like rather than a circular lumen: this is the case of the urethra according to patients' urethromethry studies by Pullan et al. (1982)[26]and Ward ans Hosker (1985)[27]. Such clinical studies included individuals with both physiological and pathological conditions, and demonstrated that in real conditions the urethra is flattened and organic tissues exert on the tube an anisotropic load rather than an isotropic external pressure. In this regard, anisotropy and inhomogeneity of soft tissues, including muscle-compressed vessels, have been proved both in physiology[28,29]and pathophysiology[30]. In particular, Cardoso et al. (2012)[29]demonstrated the anisotropy of a large variety of human soft tissues through the propagation of ultrasound waves. The authors then mathematically modelled the experimental data based on the key physical assumption that soft tissues are composed of two phases: a fluid isotropic phase formed of water and fat and an anisotropic solid tissue matrix composed of proteins and collagen. This enforces the argument of modelling soft tissue compression on vessels as composed of an isotropic part and an anisotropic one; and this condition cannot be modelled physically by a pressure chamber, nor mathematically by classical tube laws. Such experimental and clinical evidence notwithstanding, all the available mathematical models of collapsible-tube flows consider tube laws with isotropic external pressure acting on the cross-section and with circular cross-section for positive transmural pressure[11,19,20,31–35].

In this regard, the present contribution aims at providing a tube law considering a radial anisotropic external load acting on the tube, in other words we consider the external load acting anisotropically in the plane of the tube cross-section. We formulate the hypothesis, supported by clinical and experimental findings, that in physiological conditions both isotropic and anisotropic stresses are combined in the external compression acting on human vessels. Besides the analytical formulation of a new law, we performed laboratory experiments of flows in a compliant tube anisotropically loaded. The flow dynamics are also numerically simulated and the proposed tube law is tested against the experimental data. The paper is structured as follows: the methods section firstly provides a focus on the classic tube law and the version of the tube law we propose, then illustrates the laboratory activity whose data are used to test our model; the results section shows the outcomes of coupling the analytical model and the experimental data; in the discussion we examine our model compared to the classical one, we outline the model limitations and future perspectives; and, finally we draw up conclusions in the last section.

Materials and methods

The classic tube law

The tube law, also referred as "pressure-area relation", relates changes in the pipe cross-sectional area to the difference between the internal and external pressures, namely the transmural pressure, P_{tm}. The most widespread mathematical formulation of the tube law stems from the seminal work by Shapiro (1977)[19] which also analysed the solution of the tube law coupled with one-dimensional steady equations of mass and momentum conservation, introduced the speed index S, the controlling parameter of collapsible-tube flows regime defined as the ratio of flow velocity and wave speed, and mathematically explained the occurrence of flow limitation in condition of critical flow regime. The tube law in Shapiro (1977)[19], as well as in the following literature, is provided in a dimensionless form by considering the areal ratio, $\alpha = \Omega/\Omega_0$, between the current cross-section, Ω, and the reference area, i.e. the area at zero transmural pressure, Ω_0 (the subscript 0 stands for "at null P_{tm}"). The transmural pressure is made dimensionless by means of the effective stiffness of the pipe, $K = \frac{E}{12\left(1-\nu_p^2\right)}\left(\frac{2\,s}{D_0}\right)^3$, which is a combination of mechanical properties (i.e. Young modulus, E, and Poisson coefficient, ν_p) and geometrical characteristics of the tube (i.e. internal diameter, D_0, and wall thickness, s). The tube law reads[19,20,31,34]:

$$P_{tm}^{i} = \frac{(P - P_e)}{K} = \alpha^{\beta_1} - \alpha^{-\beta_2} \tag{1}$$

where P_{tm} is the dimensionless transmural pressure, P and P_e are the internal and external pressures, respectively, and β_1 and $\beta_2$are positive coefficients, typically assumed higher than 2 and equal to $3/2$, respectively[19,20,32]. In Eq. (1), the superscript i indicates isotropic conditions of external pressure, meaning that a constant pressure acts on the whole outer perimeter of the pipe, as usually dealt with in the literature[19,20,25,31–33,35]. Indeed, the tube law has been recently refined by accounting for the stenosis of the cross-section, changes in the mechanical properties of the tube-wall along the longitudinal coordinate, as well as longitudinal changes of the external pressure[31–33], though radial anisotropic external load has never been accounted for.

A basic analysis of Equation (1) shows that, for positive values of the transmural pressure (i.e. $P > P_e$), the first term on the right-hand side is predominant, the second term is negligible, and the equation provides a solution for $\alpha > 1$, only (see equation 7 in reference[20]). Conversely, when the external pressure is higher than the internal one (i.e. $P_{tm} < 0$), a solution exists for $\alpha < 1$, only, the term α^{β_1} becomes irrelevant and the behaviour is mainly governed by the second term on the right-hand side of Eq. (1). The general trend of the classic tube law is shown in figure 1 for different values of the β_1 coefficient and $\beta_2 = 3/2$. In particular, the figure shows that, for $\alpha < 1$, the behaviour is rather independent of the β_1 coefficient.

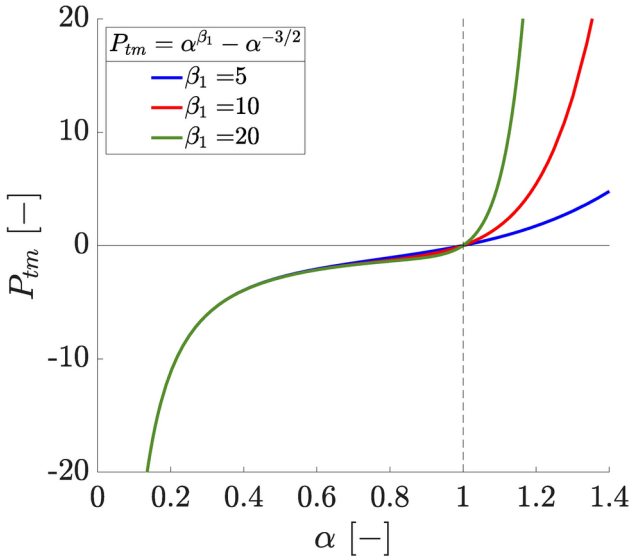

Fig. 1. The general behaviour of the tube law under isotropic conditions of external pressure for different values of the β_1 coefficient.

The tube law under anisotropic external load

The condition of anisotropic external load in the plane of the tube cross-section is typical of vessels compressed by the surrounding anisotropic tissue. In particular, the longitudinal stress acting along the tube (*x*-direction) is neglected, and only the stress tensor on the cross-section (*y*-*z* plane orthogonal to the longitudinal *x*-axis) is taken into account. Closed-form relationships for the stress components due to anisotropic load are quite cumbersome. However, in the hypothesis of small deformations, it is always possible to linearly correlate the stress tensor, σ, to the external load[36]. Additionally, in the main reference system of the pipe cross-section, the Cauchy stress tensor may be always decomposed in two stress tensors, being one isotropic (or hydrostatic) and the other one anisotropic (or deviatoric). The decomposition along the main orthogonal directions (*y*-direction with unit vector *j* and *z*-direction with unit vector *k*) yields

$$\sigma \propto \begin{pmatrix} P_j & 0 \\ 0 & P_k \end{pmatrix} = \begin{pmatrix} P_j & 0 \\ 0 & P_j \end{pmatrix} + \begin{pmatrix} 0 & 0 \\ 0 & P_k - P_j \end{pmatrix} \tag{2}$$

where P_j and P_k are the main components of the pressure-load acting along the *j*-th and *k*-th directions, respectively, on the cross-sectional plane. For the sake of clarity, in this case, we have considered $P_j < P_k$, without losing the generality of the decomposition. For isotropic external load, P_j and $P_k$are equal and the anisotropic stress tensor cancels out, such that the validity of the common pressure-area relationship holds[19]. Conversely, for anisotropic external load, we hypothesize that both the isotropic and the anisotropic stress tensors contribute to the cross-sectional deformation of the pipe. By formal analogy with the decomposition of the stress tensor (Eq. (2)), we propose the following relationship, which must be considered to be valid along the direction of maximum pressure-load (*k* in the example of Eq. (2)):

$$\begin{aligned} P_{tm} &= \frac{(P - P_e)}{K} = P_{tm}^{i} + P_{tm}^{a} = \\ &= \alpha^{\beta_1} - \alpha^{-\beta_2} + A\left(\alpha^{\beta_3} - \alpha^{-\beta_4}\right) \end{aligned} \tag{3}$$

where the superscripts i and a refer to isotropic and anisotropic, respectively, A is a coefficient depending on the external load conditions, as well as the exponents β_3 and β_4. We point out that for isotropic external pressure conditions Eq. (3) simplifies to the classic tube law (Eq.(1)), reducing to zero both the third and the fourth terms of the right-hand side of Eq. (3). Therefore, Eq. (3) provides the general formulation of the tube law under any load conditions, while still ensuring the mathematical description of collapsible tube flows under pure isotropic external pressure.

The assessment of the reference cross-sectional area Ω_0 deserves special attention when dealing with anisotropic conditions of external load. Actually a tube surrounded by a solid anisotropic medium receives an anisotropic strain, as it is the case of organic tissues compressing vessels and the direction of anisotropic stress may affect Ω_0. In this condition, a conventional choice of Ω_0 is needed, and more than one option is possible. Our choice of Ω_0 is that of the cross-section in condition of null transmural pressure; this choice prevents a direct measurement of the tube in an anisotropic medium, as illustrated in the following section and thoroughly examined in the

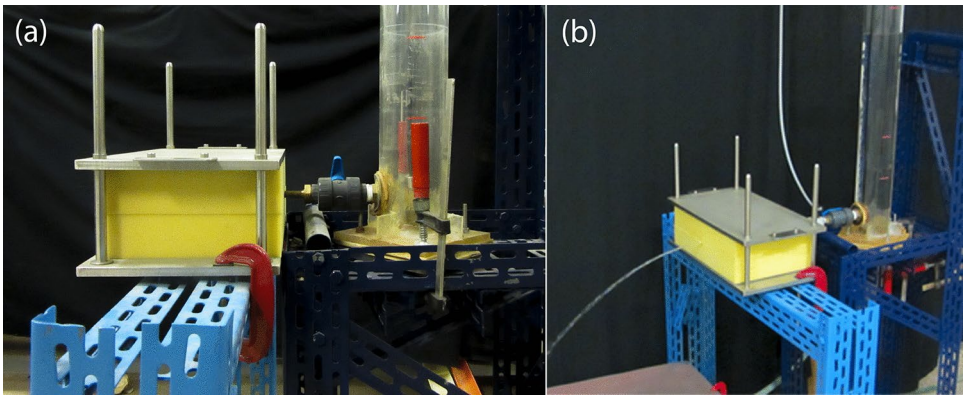

Fig. 2. A picture of the experimental setup showing the water tank connected through a valve and a rigid connector to the compressed latex tube. (**a**) A close up view of the loaded foam blocks before flow test conditions (no water in the system); (**b**) a whole view of the experimental setup during flow conditions.

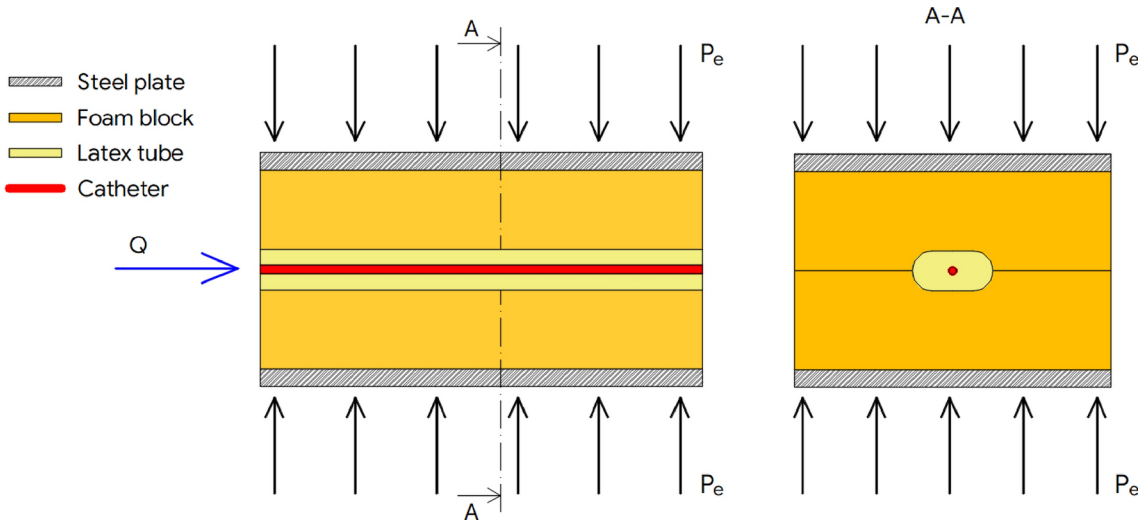

Fig. 3. A sketch of the experimental setup illustrating test conditions and the external load applied on the tube. The latex tube (yellow) is enclosed between the two rubber blocks (orange). Steel plates (gray) helped in transferring the uniform vertical load to the foam blocks and the latex tube. Red color highlights the location of the catheter, used to measured pressure head along the latex tube.

discussion, however we adopted the value of Ω_0 corresponding to $P_{tm} = 0$ in order to favour the comparison between our work and the existing literature on tube laws.

Experimental setup

To test the proposed formulation, we carried out experiments at the Fluvial and Lagoon Hydraulics and Biofluidynamics Laboratory of the Department of Civil and Environmental Engineering of the University of Florence. The experimental setup consisted of a $0.2\,m$ long collapsible pipe made of elastic latex, with an internal diameter of $5.9\,mm$. The pipe was connected to a water tank through a valve and a rigid connector (figure 2). The pipe was enclosed between two $0.30\,m$ wide and $0.05\,m$ thick foam blocks (Young's modulus, E_p, equal to $25 - 40\,kPa$) and two steel plates (figures 2 and 3), to uniformly compress the collapsible pipe and allow for anisotropic conditions of external load. The tube is simply clumped between the foam blocks, and only the vertical forces provided by the external load have been considered (figure 3). Hence, stress due to lateral confinement exerted by the foam has been neglected. Water flow rate from the tank to the pipe was controlled by a regulating valve.

In this experimental setup a direct measurement of Ω_0 at $P_{tm} = 0$ is not possible because the two foam blocks compressing the tube prevent a direct view of the tube. Instead, in experimental studies on collapsible tubes reproducing isotropic external pressure (i.e. Starling Resistor) a direct measurement of $\Omega_0$can be achieved through imaging techniques given that the tube is immersed in a fluid (e.g[22]. and[37]), Ω_0 is therefore usually measured in condition of hydrostatic intraluminal pressure equal to hydrostatic external pressure. In the anisotropic compression setup, conversely, the only direct measurement of the cross-section Ω_0 could be

achieved only before the experiments, i.e. when the tube is in an unloaded state; this possibility is outlined in the discussion. In any case, in analogy with available literature, we decided to adopt Ω_0 at null transmural pressure which corresponds to the value of the intraluminal pressure (during flow) equalling the specific value of external compression used in the experiments. This Ω_0 value has been calculated starting from measurements and computations of other quantities, precisely the total and piezometric heads, the flow velocity and the flow rate; computations from measurements as well as the mathematical model are illustrated in the "Governing equations" section.

A 6 Fr double-way catheter was placed inside the tube in order to perform flow dynamics measurements illustrated in the following of the current subsection. The presence of the catheter reduced the actual cross-section of the flow to an annular cross-section denoted Ω_0' (reported in Table 1) and obtained by subtracting the cross-sectional area of the catheter from that of the tube. Similarly to the definition of $\alpha = \Omega/\Omega_0$, we therefore introduced the annular areal ratio $\alpha' = \Omega'/\Omega_0'$; the presence of the catheter was also accounted for the computation of the hydraulic radius, $R_h' = \alpha'\Omega_0'/(\pi \cdot (D_0 + D_c))$, by considering the wetted perimeter as the sum of those of the undistorted tube and the catheter.

Our experimental setup did not mean to reproduce any apparatus in particular, yet it can be thought to be representative of flow dynamics in the lower urinary tract of the male urethra during micturition. According to this similarity, we took into account values of both the total head in the tank and the vertical load on the foam rubber blocks in the physiological ranges for the pressure in the bladder and the compression of internal organs, respectively. In this regard, we considered the usual range for pressure head values from studies on detrusorial pressure[38]and for load in the vertical direction according to ad-hoc clinical tests[11,39]. Geometrical and mechanical characteristics of the tube, the catheter and the load condition are reported in Table 1.

The emptying of the tank drove the flow inside the tube. The water level in the tank represented the total head, H_0, at the upstream inlet of the latex tube, and was measured through a pressure transducer positioned on the tank bottom recording data with a frequency of $12.5\,Hz$ corresponding to a time interval $\Delta t = 0.08\,s$. In each time interval, we measured H_0 variation, ΔH_0, whence volume variation and flow rate $Q = A \cdot \Delta H_0/\Delta t$, with A the cross-sectional area of the cylindrical tank. The value of the flow rate computed from two successive total head recordings is considered the value of the steady flow taking place in the system during that particular time interval; this quasi-steady assumption is justified later in the current section. During flow, the catheter placed inside the pipe (figure 3) has been used as a Pitot tube allowing the measurement of the piezometric head, h, and the flow velocity, U, at any cross-section along the pipe ($\Delta x = 1\,cm$). Specifically, measurements have been taken during two different runs carried out under the same initial value of the total head in the tank. In the first run the catheter was used to measure in each cross-section the "static pressure" from which the piezometric head h can be derived. In the second run the catheter has been used to measure in the same cross-sections the "dynamic pressure", so that the value of the mean flow velocity U can be obtained. Once obtained the H and h data, for each value of the initial total head in the tank, the test was performed once again in order to have useful further information of the downstream boundary: the exit velocity evaluated from the parabolic trajectory of the jet. The detection of the parabola of the jet is obtained through an image acquisition system with a digital camera and a subsequent image processing. The recorded parabolic trajectory is interpolated, thus providing the coefficients of the parabolic equation uniquely associated to the jet velocity.

For all runs, experimental conditions and the absence of constrictions along the tube entail subcritical flows only in agreement with previous studies[11]. Speed index, S, lower than 1, is of particular relevance since no transitions through critical condition ($S = 1$) occurred and thus flow limitation and elastic jump did not take place throughout the whole length of the tube[19].

Finally, the quasi-steady approximation holds because *i)* it can be assumed that the time rate of change of any variable is of the same order of magnitude as the time gradient of the emptying process, and *ii)* the time variations at a spatial location are much smaller than the spatial variation of any quantity. This condition can be mathematically expressed by rearranging the momentum equation and obtaining $\frac{1}{g}\,\frac{\partial u}{\partial t} << \frac{\partial H}{\partial x}$. We verified

Symbol	Variable	Value	Units
L	tube length	0.2	m
Ω_0	cross-section at $P_{tm} = 0$	$2.026 \cdot 10^{-5}$	m^2
Ω_0'	annular cross-section at $P_{tm} = 0$	$1.712 \cdot 10^{-5}$	m^2
s	tube thickness	$0.33 \cdot 10^{-3}$	m
E	tube elasticity modulus	$1.7 \cdot 10^6$	Pa
ϵ	tube roughness	$4.5 \cdot 10^{-5}$	m
P_e	tube compression	$5 \cdot 10^3$	Pa
D_c	catheter external diameter	$2 \cdot 10^{-3}$	m
H_0	upstream total head	$0.6 - 1.5$	m
Q	flow rate	$2.66 - 5.665$	$10^{-5}\mathrm{m}^3\mathrm{s}^{-1}$
U_e	exit flow velocity	$2.33 - 3.925$	ms^{-1}
Re	Reynolds number	$13500 - 23500$	[-]

Table 1. Summary data of physical model and experiments.

this condition through experimental measurements of the temporal variation of the outlet velocity and the total head variation between two successive sections.

Governing equations

We used experimental data of total, H, and piezometric, h, heads to calculate the flow velocity, U, and the annular areal ratio, α', according to the following well-known relationships:

$$U = \sqrt{2\,g\,(H - h)} \tag{4}$$

$$\alpha' = \frac{1}{\Omega'_0}\,\Omega' = \frac{1}{\Omega'_0}\,\frac{Q}{U} \tag{5}$$

where g is the acceleration due to gravity and Q is the flow rate. Given that Ω'_0, necessary for the computation of α' (Eq. (5)), is not achievable through direct measurements, we had to adopt an indirect assessment of Ω'_0: we computed Ω' as the ratio between Q (see the "Experimental setup" section) and U (Eq. (4)) for the specific value of piezometric head and thus internal flow pressure, $P = \gamma\,h$ (with γ, the specific weight of water), corresponding to null transmural pressure. This annular cross-section value is actually Ω'_0 (reported in Table 1) used for the nondimensionalization of each Ω' value (Eq. (5)), thus providing α' values that together with the experimental data of P_{tm} enabled us to plot our empirical tube law.

Measured and calculated data of flow pressure, P, and annular areal ratios, α', were considered for the calibration of the tube law for anisotropic external load reported in Eq. (3). The proposed pressure-area relationship (Eq. (3)) has three unknown parameters, A, β_3, and β_4, to be determined, whereas we assigned to β_1 and β_2 values that are usually adopted by classical tube laws (Eq. (1)), precisely $\beta_1 = 20$ and $\beta_2 = 3/2$[19,32,33]. Then, based on experimental data, we calibrated the coefficient A and the exponents β_3, and β_4.

The modeled quantities were calculated by solving the system consisting of the one-dimensional equations for steady flows (mass and momentum balance) and the proposed pressure-area relation for anisotropic external load (Eq. (3)). Following the hypothesis of quasi-steady flow, mass and momentum balance relationships read:

$$U\,\frac{d\Omega'}{dx} + \Omega'\,\frac{dU}{dx} = 0 \tag{6}$$

$$\frac{U}{g}\,\frac{dU}{dx} + \frac{1}{\gamma}\,\frac{dP}{dx} = -\,J \tag{7}$$

where x is the longitudinal coordinate, and J is the total head loss per unit length of the tube (i.e. the energy gradient). We involved the Darcy-Weisbach and the Colebrook-White equations as closure relationships to compute the total energy gradient, J. We solved the governing equations (3), (6) and (7) through a finite difference, single step numerical scheme with spatial discretization, dx, equal to $0.01\,m$. Due to speed index lower than 1, the system of equations was numerically solved starting from the downstream boundary condition and through an integration from downstream to upstream[32]. As boundary conditions, we considered values from experimental data in the cross-sections at $x = 0.18\,m$. *Predicted values* (obtained from numerical integration of Eq.s (3), (6) and (7)) were compared to *experimental data* (measured and derived from measurements through Eq.s (4) and (5)) in a reduced length of the pipe ($x = 0.06 - 0.18\,m$), to avoid disturbances introduced by boundary conditions (i.e. the presence of the upstream rigid connector and the downstream free jet outside the foam block)[32].

We compared predicted and experimental data in terms of mean flow velocity, U, piezometric head, $h = P/\gamma$, and total head, H, according to flow conditions (i.e. flow rate or transmural pressure). Lastly, we compared the proposed tube law against experimental data of transmural pressure and annular areal ratio, α'. We measured the goodness of data fitting in terms of the Root Mean Square Error (RMSE).

Results

In Eq. (3) the "isotropic part" of the tube law, namely the first and second terms of the equation, was not object of calibration and we adopted the exponents values provided by literature. Conversely, we calibrated the parameters A, β_3 and β_4 characterizing the "anisotropic part" (third and fourth terms) of Eq. (3). We found that, for the range of anisotropic transmural pressure measured in the performed experiments, both the coefficient A (figure 4a) and the exponents β_3 and β_4 (figures 4b and 4c respectively) may be related to the values of P_{tm} occurring in the downstream cross-section of the collapsible pipe. The reason behind this correlation is pretty straightforward: the downstream cross-section is taken into account to set boundary conditions for modelling, given that all our experiments ran in subcritical condition. Based on this consideration, the transmural pressure can be easily calculated in such boundary section, and accordingly, the parameters A, β_3 and β_4 can be easily retrieved from calibrated relationships. Indeed, figure 4 illustrates the behaviour of parameters A, β_3 and β_4 as a function of the pressure measured at the downstream end of the modeled tract of the tube, labelled P_{tm}^{DS}; in this section (namely $x = 0.18\,m$ in our experimental setup) the transmural pressure has the minimum value recorded along the tube in accordance to the conditions of subcritical flow for which internal pressure and cross-sectional area decrease in the downstream direction, whereas flow velocity increases[19]. In particular, figure 4a

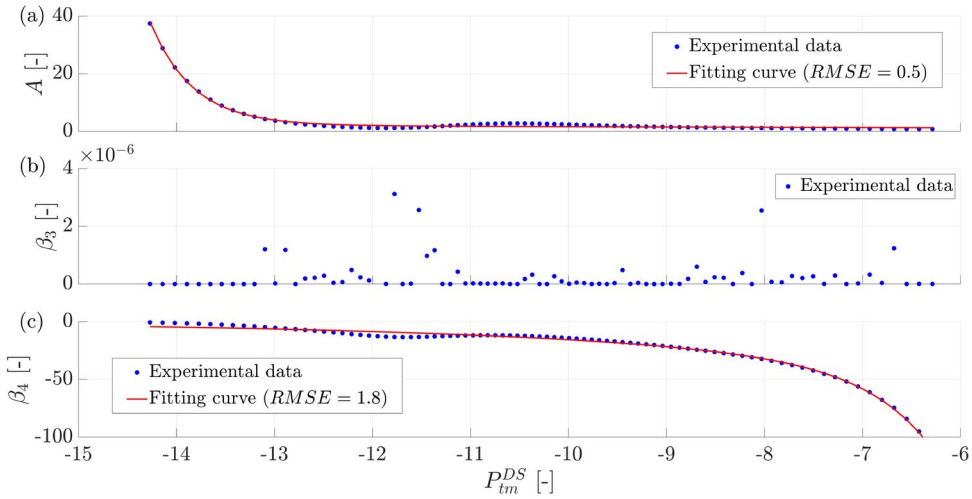

Fig. 4. The coefficient A, panel (**a**) and the exponents β_3 and β_4, panel (**b**) and (**c**) respectively, as a function of the downstream transmural pressure. The root mean square error (RMSE) of the fitting curves is provided for A and β_4.

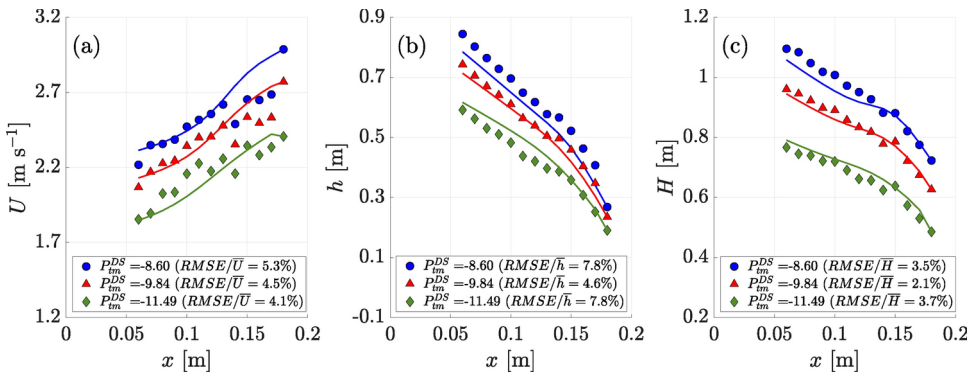

Fig. 5. Integration profiles of the flow characteristics in the simulated tract of the tube for three different values of the downstream transmural pressure ($P_{tm}^{DS} = -8.60$ in blue, $P_{tm}^{DS} = -9.84$ in red, $P_{tm}^{DS} = -11.49$ in green). Measured values from experiments are represented by circles, triangles and diamonds, respectively, and corresponding colors. Percentage root mean square error (*RMSE*) is given for each profile. (**a**) Measured values and integration profiles of the mean flow velocity, U; (**b**) Measured values and integration profiles of the piezometric head, h; (**c**) Measured values and integration profiles of the total head, H.

shows that in the range of $P_{tm}^{DS} < 0$, the lower is the transmural pressure the more relevant is the coefficient A; irrespective of any transmural pressure value, the exponent β_3 is negligible (figure 4b); in the range of $P_{tm}^{DS} < 0$, the lower is the transmural pressure the less relevant is the exponent β_4 (figure 4c). The meaning and the effect of such behaviour will be illustrated in the discussion by means of the plot of the tube law with these calibrated parameters represented together with the experimental points (figure 6b).

Once the tube law was calibrated, we coupled Eq. (3) to the mass and momentum balance relationships (Eqs. (6) and (7)) to model the experimental flows. The comparison between experimental and predicted values are shown in figure 5 for selected data. For the sake of brevity, the comparison is shown for three values of the total head, H_0, in the tank, which corresponds to three different values of the transmural pressure at the downstream boundary cross-section, P_{tm}^{DS} (namely at $x = 0.18\,m$).

Figure 5 shows the experimental data for flow velocity, U, piezometric head, h, and total head, H, for three experiments with initial total head $H_0 = 1.2\,m$, corresponding to $P_{tm}^{DS} = -8.60$ (blue circles); $H_0 = 1.05\,m$, corresponding to $P_{tm}^{DS} = -9.84$ (red triangles); and $H_0 = 0.9\,m$, corresponding to $P_{tm}^{DS} = -11.49$ (green diamonds), respectively. For the same experimental conditions, figure 5 shows the resulting integration profiles (predicted values). We recall that the experimental outputs in figure 5 result from direct measurements of the total head, H, and the piezometric head, h, by the catheter and from computations of the flow velocity (Eq. (4)).

Figure 5 shows an overall good agreement between the predicted values and the experimental points considered. The root mean square error (RMSE) is well below 10% for all the considered variables. More specifically, the RMSE is even lower (in the order of 3%–4%) for the flow velocity, U, and the total head, H. While the RMSE is slightly higher for the piezometric head, h, with a maximum value of 7.8% for the tested

values of $P_{tm}^{DS} = -8.60$ and $P_{tm}^{DS} = -11.49$ (figure 5b). As a result, the proposed tube law (Eq. (3)) seems to well describe the compliant behaviour of a collapsible tube in the simulated flow conditions.

Discussion

Firstly, we will discuss the assessment of the undisturbed cross-sectional area Ω_0. On one hand, as far as isotropic load conditions are concerned, the reference area, Ω_0, is usually and straightforwardly measured at $P_{tm} = 0$ [16,24]. Such a condition may be obtained for, mathematically speaking, infinite combinations of the internal and the external pressures, provided the requirement $P = P_e$ is satisfied. Regardless of the particular (P, P_e) load combination, it is, however, mathematically reasonable to suppose the existence of a unique value of the reference cross-sectional area. On the other hand, it physically makes sense to presume that at any anisotropic value and configuration of external load (equalling the internal pressure) a specific cross-sectional area is retrieved. In this condition, for each value $P = P_e$ a specific cross-sectional area characterizes the tube depending on the intensity and the direction of the anisotropic stress, as we will show in the following of this discussion. That being said, it is however convenient to define a reference Ω_0, the choice of which cannot but be arbitrary. As illustrated in the first three subsections of the methods, in our anisotropic external load conditions we adopted Ω_0 at null P_{tm} to favour the comparison with isotropic external pressure studies, even if in our case this choice of Ω_0 required indirect calculations. Alternatively a practical value of Ω_0 could be directly measured when the tube is in unloaded conditions (outside the foam blocks); by means of high resolution photos we retrieved such cross-sectional area ($27.57\,mm^2$) from which by subtracting the catheter cross-sectional area is possible to obtain an alternative reference annular cross-section. This alternative choice of Ω_0 would be indeed functional and represent the measurement carried out for null internal and external relative pressure. Actually, both in experimental and clinical settings, it is much more handy to use the reference cross-sectional area obtained measuring the tube or the vessel outside the experimental apparatus or the organic tissue, and it would be practical to adopt this convention both for anisotropic and isotropic medium surrounding the tube, since this choice represents a clear added value in terms of convenience and functionality. However, one must be aware that the Ω_0 value at $P = P_e = 0$ is higher than the Ω_0 value at $P = P_e$ equalling the specific anisotropic load, as in our case where Ω_0 at $P = P_e = 0$ is $27.57\,mm^2$, larger than $20.26\,mm^2$, namely Ω_0 at $P = P_e =$ compression load (see Table 1). For the tube law plotted in figure 6b) the second value is used (Ω_0 at $P = P_e =$ compression load); using alternatively Ω_0 at $P = P_e = 0$ would entail a horizontal shift of the tube law plot in the $\alpha - P_{tm}$ plane.

The representation of the tube law obtained with the Ω_0 value at $P = P_e$ equalling the specific anisotropic load is provided in figure 6. We represented in the $\alpha' - P_{tm}$ plane both the experimental data and the theoretical tube laws with the aim of analysing the behaviour of the classic tube law (Eq. (1)) and the proposed pressure-area relationship (Eq. (3)). The performance in fitting experimental data collected from tests in conditions of vertical compression of the tube is graphically depicted in figure 6 for both the classic and the proposed tube laws. In both panels of figure 6 we considered a selection of the total amount of experimental points: this selection is the same represented for the integration profiles illustrated in figure 5; for the sake of clarity the legend reports the three values of downstream transmural pressure identifying the three selected tests.

In figure 6a the classic tube law is graphed by the thick black line representing the plot of Eq. (1) with $\beta_1 = 20$ and $\beta_2 = 3/2$ as well as the experimental data of the tests carried out under condition of anisotropic external load. Alongside the experimental points, figure 6b also shows the graphical trend of the corresponding curves of the pressure-area relationship: the three curves are the plots of Eq. (3) with different values of the parameters A, β_3 and β_4 as a function of P_{tm}^{DS}, according to the calibration illustrated in the results.

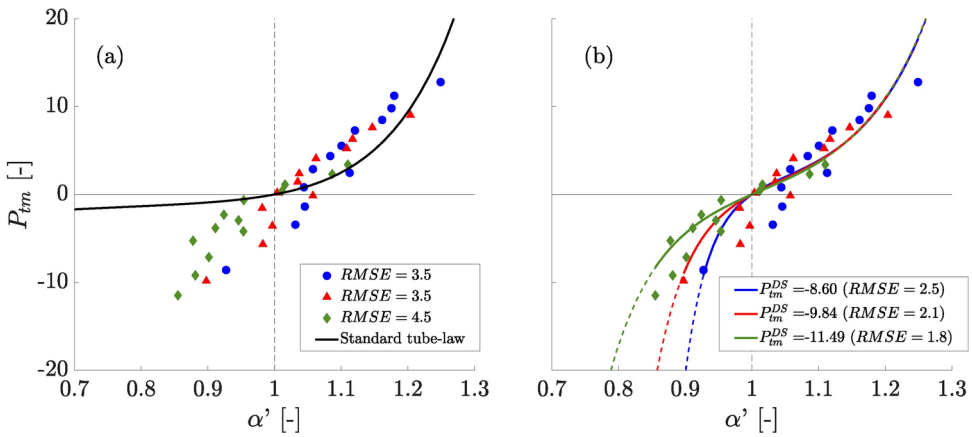

Fig. 6. Comparison between experimental values of the transmural pressure P_{tm} and the annular cross-section α' for some performed tests and theoretical and empirical tube-laws represented by solid lines for the experimental data range and dashed lines for extrapolation. (**a**) Comparison of three performed experiments with different downstream transmural pressure, P_{tm}^{DS} with (**a**) the classic tube law (Eq.(1)) and (**b**) the proposed tube-law (Eq. (3)).

The comparison of the classic and proposed tube laws in experimental fitting performance reveals that the classic tube law catches quite well the experimental data in the positive range of P_{tm}, but definitely not for $P_{tm} < 0$; instead, the fitting of the proposed tube law better performs both for first and third quadrants. In particular, for the curve limb in the upper right quadrant the relevant terms of Eq. (3) are the first and and third one, and the calibration of A and β_3 provides a balancing of the third term of Eq. (3) on the first one; this adjusts the positive limb of the tube law with a better fitting of the graph in the first quadrant in panel 6b with respect to panel 6a. Comparing the bottom left quadrant of panels a) and b) we observe that the classic tube law does not describe adequately the experimental results since it predicts large cross-section changes for small transmural pressure changes, whereas experimental points are well below the *x*-axis and thus distant from the plot limb for negative transmural pressure, which definitely has a small inclination in disagreement with empirical data. Instead the proposed tube law (panel b) curves) catches also in third quadrant the empirical (α', P_{tm}) points; this is mainly due to the third term of Eq. (3) characterized by the exponent β_4 (figure 4c) which is negative with an increasing absolute value with decreasing transmural pressure. This influences the first term of Eq. (3), being the first and third terms the governing ones for $P_{tm} < 0$, the third term modifies the inclination of the limb of the bottom left quadrant, the lower the transmural pressure the higher the inclination (in accordance with the behaviour of β_4 as a function of P_{tm}^{DS}).

Moreover, the presence of tangential stresses on the outer surface of the collapsible tube is usually negligible compared to the stress induced by internal and external pressure (i.e. transmural pressure) when the deformation of the cross-section is considered[40]. Even the contribution given by the weight of the pipe itself appears to be negligible. The transmural pressure induced by pipe weight, P_{tm}^{w}, can be calculated to be in the order of

$$P_{tm}^{w} \approx \rho_p \; g \; \frac{\pi \; D \; s}{K} \tag{8}$$

where ρ_p is the density of the pipe material, D is the pipe diameter, s is the pipe thickness. For common values of rubber density, the self-induced transmural pressure appears to be at least 3 orders of magnitude lower than the values of transmural pressure induced by internal pressure of flow.

Besides, in our case also the pipe eccentricity, due to its own weight, was negligible as it usually is for small tubes unlike larger pipes such as those analysed by[22] in which elliptical configuration at rest may play a role.

Finally, an additional validation of our model through its application to experimental and and clinical data of cited researches[26]and[27] on the urethra was not possible since both studies do not provide complete data on cross-sectional area of the conduit, transmural pressure and flow velocity in the conduit. By using both radiological and histological methods, Pullan et al.[26]substantiate the slit-like shape of the urethral cross-section, thus suggesting the complex distribution of the external load acting on the conduit, however the study does not provide flow measurements and transmural pressures. Ward and Hosker[27]demonstrate that occlusive forces acting on the urethra are anisotropic, but the authors do not couple such data with cross-sectional area measurements. Though, the proposed tube law for anisotropic external load can be of clinical relevance. Based on suitable measurements, we proved that the proposed 1D model is able to catch the effects induced by anisotropic external load on compliant vessels. Compared to more complex 3D constitutive laws (for instance[41]and[42]) a simple 1D model appears to be more reliable and ready to use in real case applications.

Conclusions

In this work we proposed a new version of the tube law for collapsible-tube flows under conditions of external load acting anisotropically in the plane of the tube cross-section, since clinical and experimental observations show that in human physiology both isotropic and anisotropic stresses are combined in the external pressure acting on vessels. Tube laws found in literature, however, only account for isotropic conditions of external pressure. Moreover, such tube laws are not tested against experimental data reproducing flows taking place in compliant tubes subject to compression varying in space as it is attested in lifelike conditions: either mathematical modeling of collapsible-tube flows found in literature remains purely theoretical or perform laboratory observations in static conditions only. To overcome this gaps we formulated a new physically based tube law and carried out laboratory tests reproducing collapsible-tube flows under conditions of unidirectional tube compression. The tube law, calibrated through the experimental data, was included in the system of governing equation to simulate the flows of the laboratory tests; we achieved very good agreement between the experimental points and the integration profiles. The experimental data and the mathematical prediction of both the classic and empirical tube laws were compared in the $\alpha - P_{tm}$ plane.

The empirical tube law presents a similar trend of the classic tube law in the upper right quadrant, and a quite different trend in the bottom left quadrant; in both cases our proposed tube law provides a very good fitting of the experimental data, much better than the classic tube law. Unlike the classic pressure-area relationship, the empirical tube law for conditions of anisotropic external pressure P_e cannot rely on a single, univocal value of Ω_0 at $P_{tm} = 0$ regardless the specific $P = P_e$ value, so that the choice of Ω_0 cannot but be arbitrary. We adopted as Ω_0 the measurement obtained at $P = P_e$ equalling the specific external vertical compression characterizing our experiments, even if this is not a direct measurement because the anisotropic medium surrounding the tube makes it not visible. We therefore argued that an Ω_0 value in condition of $P = P_e = 0$ could be the easiest and handiest choice. Indeed, the novel experimental field of collapsible tube flows under anisotropic external load comes at a price: limitation in cross-sectional measurements including Ω_0.

Data availability

The datasets generated and analysed during the current study are available from the corresponding author on reasonable request.

Received: 13 August 2024; Accepted: 5 December 2024
Published online: 17 December 2024

References

1. Pedley, T. J. Blood flow in arteries and veins, pp. 105–158. Cambridge University Press, ??? (2000)
2. Carpenter, P. W. & Pedley, T. J. Flow past highly compliant boundaries and in collapsible tubes. In: Proceedings of the IUTAM Symposium Held at the University of Warwick . https://doi.org/10.1007/978-94-017-0415-1. Springer (2001)
3. Laudato, M., Mosca, R. & Mihaescu, M. Buckling critical pressures in collapsible tubes relevant for biomedical flows. *Scientific Reports*. **13**(9298 (2023)) (2023) https://doi.org/10.1038/s41598-023-36513-6.
4. Kamm, R. D. & Pedley, T. J. Flow in collapsible tubes: A brief review. *Journal of Biomechanical Engineering*. **111**(3), 177–179. https://doi.org/10.1115/1.3168362 (1989).
5. Laudato, M. & Mihaescu, M. Analysis of the contact critical pressure of collapsible tubes for biomedical applications. *Continuum Mechanics and Thermodynamicsy*. **36**, 217–228 (2024) https://doi.org/10.1007/s00161-023-01271-3
6. Hoffman, J. & Spaan, J. Pressure-flow relations in coronary circulation. *Physiological reviews*. **70**(2), 331–390. https://doi.org/10.1152/physrev.1990.70.2.331 (1990).
7. Pedley, T. J., Brook, B. S. & Seymour, R. S. Blood pressure and flow rate in the giraffe jugular vein. Philosophical Transactions of the Royal Society of London. Series B: Biological Sciences **351**(1342), 855–866. https://doi.org/10.1098/rstb.1996.0080 (1996).
8. Elad, D. & Kamm, R. D. Parametric evaluation of forced expiration using a numerical model. *Journal of Biomechanical Engineering*. **111**(3), 192–199. https://doi.org/10.1115/1.3168365 (1989).
9. Hyatt, R. E. Forced Expiration, pp. 295–314. John Wiley & Sons, Ltd, ???. https://doi.org/10.1002/cphy.cp030319 (2011).
10. Wilson, T. A., Rodarte, J. R. & Butler, J. P. Wave-Speed and Viscous Flow Limitation, pp. 55–61. John Wiley & Sons, Ltd, ??? https://doi.org/10.1002/cphy.cp030305 (2011).
11. Griffiths, D. Hydrodynamics of male micturition—i theory of steady flow through elastic-walled tubes. *Medical and Biological Engineering*. **9**(6), 581–588. https://doi.org/10.1007/BF02474637 (1971).
12. Patterson, S. & Starling, E. On the mechanical factors which determine the output of the ventricles. *The Journal of physiology*. **48**(5), 357–379. https://doi.org/10.1113/jphysiol.1914.sp001669 (1914).
13. Kamm, R. D. & Shapiro, A. H. Unsteady flow in a collapsible tube subjected to external pressure or body forces. *Journal of Fluid Mechanics*. **95**(1), 1–78. https://doi.org/10.1017/S0022112079001348 (1979).
14. Katz, A. I., Chen, Y. & Moreno, A. H. Flow through a collapsible tube: experimental analysis and mathematical model. *Biophysical Journal*. **9**(10), 1261–1279. https://doi.org/10.1016/S0006-3495(69)86451-9 (1969).
15. Bertram, C. D., Raymond, C. J. & Butcher, K. S. Oscillations in a collapsed-tube analog of the brachial artery under a sphygmomanometer cuff. *Journal of biomechanical engineering*. **111**(3), 185–191. https://doi.org/10.1115/1.3168364 (1989).
16. Bertram, C. The effects of wall thickness, axial strain and end proximity on the pressure-area relation of collapsible tubes. *Journal of biomechanics*. **20**(9), 863–876. https://doi.org/10.1016/0021-9290(87)90146-1 (1987).
17. Scroggs, R. A., Beck, S. B. M. & Patterson, E. A. An integrated approach to modelling the fluid-structure interaction of a collapsible tube. *JSME International Journal Series B Fluids and Thermal Engineering*. **47**(1), 20–28. https://doi.org/10.1299/jsmeb.47.20 (2004).
18. Lambert, R. K. & Wilson, T. A. Flow limitation in a collapsible tube. *Journal of applied physiology*. **33**(1), 150–153. https://doi.org/10.1152/jappl.1972.33.1.150 (1972).
19. Shapiro, A. H. Steady flow in collapsible tubes. *Journal of Biomechanical Engineering*. **99**(3), 126–147. https://doi.org/10.1115/1.3426281 (1977).
20. Elad, D., Kamm, R. D. & Shapiro, A. H. Choking phenomena in a lung-like model. *Journal of biomechanical engineering*. **109**(1), 1–9. https://doi.org/10.1115/1.3138636 (1987).
21. Bonis, M. & Ribreau, C. Wave Speed in Noncircular Collapsible Ducts. *Journal of Biomechanical Engineering*. **103**(1), 27–31. https://doi.org/10.1115/1.3138241 (1981).
22. Bertram, C. & Ribreau, C. Cross-sectional area measurement in collapsed tubes using the transformer principle. *Journal of Medical and Biological Engineering and Computing*. **27**, 357–364. https://doi.org/10.1007/BF02441426 (1987).
23. Ribreau, C., Naili, S., Bonis, M. & Langlet, A. Collapse of Thin-Walled Elliptical Tubes for High Values of Major-to-Minor Axis Ratio. *Journal of Biomechanical Engineering*. **115**(4A), 432–440. https://doi.org/10.1115/1.2895508 (1993).
24. Thiriet, M. & Ribreau, C. Computational flow in a collapsed tube with wall contact. *Mécanique & Industries*. **1**(4), 349–364 (2000).
25. Drzewiecki, G., Field, S., Moubarak, I. & Li, J.K.-J. Vessel growth and collapsible pressure-area relationship. *American Journal of Physiology-Heart and Circulatory Physiology*. **273**(4), 2030–2043. https://doi.org/10.1152/ajpheart.1997.273.4.H2030 (1997).
26. Pullan, B., Phillips, J. & Hickey, D. Urethral lumen cross-sectional shape: its radiological determination and relationship to function. *British journal of urology*. **54**(4), 399–407. https://doi.org/10.1111/j.1464-410x.1982.tb08953.x (1982).
27. Ward, G. & Hosker, G. The anisotropic nature of urethral occlusive forces. BJOG: An International Journal of Obstetrics & Gynaecology **92**(12), 1279–1285 (1985) https://doi.org/10.1111/j.1471-0528.1985.tb04876.x
28. Sander, E. A., Stylianopoulos, T., Tranquillo, R. T. & Barocas, V. H. Image-based biomechanics of collagen-based tissue equivalents. *IEEE Engineering in Medicine and Biology Magazine*. **28**(3), 10–18. https://doi.org/10.1109/MEMB.2009.932486 (2009).
29. Cardoso, L. & Cowin, S. C. Role of structural anisotropy of biological tissues in poroelastic wave propagation. *Mechanics of Materials*. **44**, 174–188 (2012) https://doi.org/10.1016/j.mechmat.2011.08.007
30. Jain, R. K., Martin, J. D. & Stylianopoulos, T. The role of mechanical forces in tumor growth and therapy. *Annual Review of Biomedical Engineering*. **16**(1), 321–346. https://doi.org/10.1146/annurev-bioeng-071813-105259 (2014).
31. Toro, E. F. & Siviglia, A. Flow in collapsible tubes with discontinuous mechanical properties: mathematical model and exact solutions. *Communications in Computational Physics*. **13**(2), 361–385. https://doi.org/10.4208/cicp.210611.240212a (2013).
32. Siviglia, A. & Toffolon, M. Steady analysis of transcritical flows in collapsible tubes with discontinuous mechanical properties: implications for arteries and veins. Journal of fluid mechanics **736**, 195–215 https://doi.org/10.1017/jfm.2013.542 (2013).
33. Siviglia, A. & Toffolon, M. Multiple states for flow through a collapsible tube with discontinuities. Journal of fluid mechanics **761**, 105–122 https://doi.org/10.1017/jfm.2014.635 (2014).
34. Müller, L. O. & Toro, E. F. A global multiscale mathematical model for the human circulation with emphasis on the venous system. *International journal for numerical methods in biomedical engineering*. **30**(7), 681–725. https://doi.org/10.1002/cnm.2622 (2014).
35. Kozlovsky, P., Zaretsky, U., Jaffa, A. J. & Elad, D. General tube law for collapsible thin and thick-wall tubes. *Journal of Biomechanics*. **47**(10), 2378–2384. https://doi.org/10.1016/j.jbiomech.2014.04.033 (2014).
36. Melworm, R. F., Patel, P. D. & Berman, I. Shell Theory Solution for Asymmetric Balanced Radial Loads on Long Cylinders. *Journal of Engineering for Power*. **90**(2), 177–185. https://doi.org/10.1115/1.3609160 (1968).
37. Kamimura, T., Ohba, K. & Band, K. Two-dimensional numerical simulation and experiment on large deformation of collapsible tube. *JSME International Journal Series C*. **43**(4), 889–894. https://doi.org/10.1299/jsmec.43.889 (2000).

38. Abrams, P. & Griffiths, D. The assessment of prostatic obstruction from urodynamic measurements and from residual urine. *British Journal of Urology*. **51**(2), 129–134. https://doi.org/10.1111/j.1464-410x.1979.tb02846.x (1979).
39. Brown, M. & Wickham, J. The urethral pressure profile. *British Journal of Urology*. **41**(2), 211–217. https://doi.org/10.1111/j.1464-410x.1969.tb09925.x (1969).
40. Tang, D., Yang, C., Walker, H., Kobayashi, S. & Ku, D. N. Simulating cyclic artery compression using a 3d unsteady model with fluid-structure interactions. *Computers & Structures*. **80**(20–21), 1651–1665. https://doi.org/10.1016/S0045-7949(02)00111-6 (2002).
41. Gasser, T. C., Ogden, R. W. & Holzapfel, G. A. Hyperelastic modelling of arterial layers with distributed collagen fibre orientations. *Journal of The Royal Society Interface*. **3**(6), 15–35. https://doi.org/10.1098/rsif.2005.0073 (2006).
42. Kamenskiy, A. V. et al. Biaxial mechanical properties of the human thoracic and abdominal aorta, common carotid, subclavian, renal and common iliac arteries. *Biomechanics and Modeling in Mechanobiology*. **13**, 1341–1359 https://doi.org/10.1007/s10237-014-0576-6 (2014).

Acknowledgements
The authors are thankful to Mauro Gioli and Muzio Mascherini of the laboratory technical staff for their support in implementing the physical model; the authors also thank the B.Sc. and M.Sc. students who helped running the experiments.

Author contributions
Lorenzo Lotti carried out the experimental activity, post-processed and analysed the data, formulated the empirical tube law, and partly drew up some plots; he also revised the manuscript after writing completion. Costanza Carbonari analysed the dataset, formulated the empirical tube law, partly carried out numerical computation and wrote the manuscript. Giulio Calvani analysed the dataset, formulated the empirical tube law, carried out numerical computation, and partly drew up some plots; he also revised the manuscript after writing completion. Enio Paris supervised all the steps of this research and revised the manuscript after writing completion.

Declarations

Competing interests
The authors declare no competing interests.

Additional information
Correspondence and requests for materials should be addressed to C.C.

Reprints and permissions information is available at www.nature.com/reprints.

Publisher's note Springer Nature remains neutral with regard to jurisdictional claims in published maps and institutional affiliations.

Open Access This article is licensed under a Creative Commons Attribution-NonCommercial-NoDerivatives 4.0 International License, which permits any non-commercial use, sharing, distribution and reproduction in any medium or format, as long as you give appropriate credit to the original author(s) and the source, provide a link to the Creative Commons licence, and indicate if you modified the licensed material. You do not have permission under this licence to share adapted material derived from this article or parts of it. The images or other third party material in this article are included in the article's Creative Commons licence, unless indicated otherwise in a credit line to the material. If material is not included in the article's Creative Commons licence and your intended use is not permitted by statutory regulation or exceeds the permitted use, you will need to obtain permission directly from the copyright holder. To view a copy of this licence, visit http://creativecommons.org/licenses/by-nc-nd/4.0/.

© The Author(s) 2024